Solar Energy Materials & Solar Cells 159 (2017) 227–234

Contents lists available at ScienceDirect

Solar Energy Materials & Solar Cells

journal homepage: www.elsevier.com/locate/solmat

From unstable $CsSnI_3$ to air-stable Cs_2SnI_6: A lead-free perovskite solar cell light absorber with bandgap of 1.48 eV and high absorption coefficient

Xiaofeng Qiu [a], Bingqiang Cao [a,*], Shuai Yuan [a], Xiangfeng Chen [a], Zhiwen Qiu [a], Yanan Jiang [a], Qian Ye [b], Hongqiang Wang [b,*], Haibo Zeng [c], Jian Liu [d], Mercouri G. Kanatzidis [d,*]

[a] Materials Research Center for Energy and Photoelectrochemical Conversion, School of Material Science and Engineering, University of Jinan, Jinan 250022, China
[b] Center for Nano Energy Materials, School of Materials Science and Engineering, Northwestern Polytechnical University, Xi'an 710072, China
[c] Institute of Optoelectronics and Nanomaterials, School of Materials Science and Engineering, Nanjing University of Science and Technology, Nanjing 210094, China
[d] Department of Chemistry, Northwestern University, Evanston, IL 60208, United States

ARTICLE INFO

Article history:
Received 14 May 2016
Received in revised form
1 September 2016
Accepted 16 September 2016
Available online 22 September 2016

Keywords:
Perovskite absorber
Air-stable
Lead-free
Cs_2SnI_6
Solar cell

ABSTRACT

All-inorganic and lead-free cesium tin halides ($CsSnX_3$, X=Cl, Br, I) are highly desirable for substituting the organolead halide perovskite solar cells. However, the poor stability of $CsSnX_3$ perovskites has so far prevented the fabrication of devices that can withstand sustained operation under normal conditions. In this paper, a two-step sequential deposition method is developed to grow high-quality B-γ-$CsSnI_3$ thin films and their unique phase change in atmosphere is explored in detail. We find the spontaneous oxidative conversion from unstable B-γ-$CsSnI_3$ to air-stable Cs_2SnI_6 in air. Allowing the phase conversion of the $CsSnI_3$ film to evolve in ambient air it gives the semiconducting perovskite Cs_2SnI_6 with a bandgap of 1.48 eV and high absorption coefficient (over 10^5 cm^{-1} from 1.7 eV). More importantly, the Cs_2SnI_6 film, for the first time, is adopted as a light absorber layer for a lead-free perovskite solar cell and a preliminary estimate of the power conversion efficiency (PCE) about 1% with open-circuit voltage of 0.51 V and short-circuit current of 5.41 mA/cm^2 is realized by optimizing the perovskite absorber thickness. According to the bandgap and the Shockley-Queisser limit, such inorganic perovskite solar cell with higher efficiency and pronounced stability can be expected by material quality improvement and device engineering.

1. Introduction

Halide perovskite semiconductors are attracting more attention due to their new outstanding photovoltaic and potentially inexpensive fabrication technology [1–5]. For example, the methylammonium lead iodide ($CH_3NH_3PbI_3$) perovskite is an excellent light harvester and has enabled major progress [6–8], since Miyasaka et al. reported the perovskite-sensitized solar cells as a variant of the dye-sensitized solar cell (DSSC) configuration [9]. Following the initial reports of all-solid lead halide perovskite solar cells with efficiencies of 10–11% [10,11], a rapid succession of the efficiency race has led to its rise over 20% [12]. Both methylammonium and cesium lead halide perovskites (MA/$CsPbX_3$, X=Cl, Br, I) nanocrystals also have been reported with narrow size distributions, high photoluminescence quantum yield up to 90%, and wide color gamut, which are also very interesting for solid light emitting [13–17]. For developing perovskite solar cells, related endeavors are now currently focusing on pursuing of higher device efficiency and seeking solutions over the instability of the perovskite light absorber. Meanwhile, the consideration over the toxicity of lead (Pb) in the lead halide perovskite solar cells has stimulated the search for lead-free solar cells [18], in which $CsSnX_3$ perovskites are promising candidates, especially for $CsSnI_3$ due to the similar semiconductor properties [19–21]. Chung et al. [22] reported that $CsSnI_3$ was a good solid state electrolyte for DSSC with high photovoltaic efficiency (10.2%) but the underlying working mechanism is still controversial [23]. A Schottky solar cell based on $CsSnI_3$ thin-film exhibited an efficiency of 0.44% under light illumination of 50 mW/cm^2 [24]. Kumar et al. [25]

* Corresponding authors.
E-mail addresses: mse_caobq@ujn.edu.cn (B. Cao), hongqiang.wang@nwpu.edu.cn (H. Wang), m-kanatzidis@northwestern.edu (M.G. Kanatzidis).

http://dx.doi.org/10.1016/j.solmat.2016.09.022
0927-0248/

demonstrated that high photocurrents (~20 mA/cm^2) of TiO_2-based mesoporous solar cell with $CsSnI_3$ as active layer can be obtained through vacancy modulation. However, the device fabrication and testing were all done in nitrogen filled glovebox to prevent the fast fail due to the severe instability of $CsSnI_3$.

Therefore, although lead-free cesium tin halides ($CsSnX_3$, X=Cl, Br, I) are highly desirable for substituting the organolead halide perovskite solar cells, the poor stability of $CsSnX_3$ perovskites has so far prevented the fabrication of devices that can withstand sustained operation under ambient air conditions. Herein, we report an encouraging discovery that B-γ-$CsSnI_3$ film can spontaneously converts in air and at room temperature to an air-stable Cs_2SnI_6 film, which can be adopted as lead-free solar cell light absorber owing to its direct bandgap of 1.48 eV and high absorption coefficient (over 10^5 cm^{-1} from 1.7 eV). We have further exploited its use in a N-i-P planar solar cell by utilizing such Cs_2SnI_6 film as the light absorber, and achieved currently a conversion efficiency of near 1% in air, which is comparable to that of reported $CsSnI_3$ cells in the nitrogen glove box [25], but with very promising promotion by future efforts of device engineering. Our study thus underscores new possibilities for developing lead-free perovskite solar cells with high efficiency and pronounced stability.

2. Experimental methods

Synthesis of B-γ $CsSnI_3$ and Cs_2SnI_6 The B-γ-$CsSnI_3$ thin film was synthesized on glass substrates through a two-step method, that is, vapor deposition followed by solid-state reaction. Prior to thermal evaporation, glasses were cleaned with ethanol, isopropanol and acetone (volume ratio 1:1:1) by ultrasonication treatment. Then CsI (99.9%, Aladdin) and SnI_2 (99+%, Alfa Aesar) layers with the same thickness (250 nm) were successively deposited on the glass substrates using thermal evaporation, followed by rapid annealing (190–330 °C for 1800 s) under N_2 atmosphere to complete the solid state reaction between the layers. The growth rates of CsI and SnI_2 vary from 0.5 to 1 Å. Finally, when it was cooled to 80 °C naturally, fresh B-γ-$CsSnI_3$ thin films with black color were obtained. In air, the B-γ-$CsSnI_3$ thin film will change to Cs_2SnI_6 film automatically by phase change. We name CI/SI film and SI/CI film simply as the films grown with CsI/SnI_2 and SnI_2/CsI deposition order, respectively.

Device fabrication of Cs_2SnI_6 based solar cell The devices were prepared on cleaned Fluorine-doped tin oxide (FTO) glass substrates. FTO glass (20 Ω/□) was first etched off a strip of conductive area on the edge side by HCl and Zn powders. The etched substrates were then sequentially cleaned in soap water, acetone, deionized water, and ethanol in ultrasonic bath, and then dried under argon flow, followed by putting the cleaned FTO in 0.2 M $TiCl_4$ solution at 70 °C for one hour to prepare the compact-TiO_2 (c-TiO_2) blocking layer. The Cs_2SnI_6 thin film was prepared by phase change of B-γ-$CsSnI_3$ film deposited on FTO-glass substrate in air. Then, hole transport layer composed of 10 mg poly(3-hexylthiophene) (P3HT) dissolved in 1 mL of chlorobenzene was spin-coated onto the Cs_2SnI_6 film at 2000 rpm for 30 s. Finally, 80 nm of Ag as back contact was deposited through thermal evaporation. For each group devices, 5–10 solar cells were successfully fabricated for device performance and reproducibility evaluation.

Materials and device characterization X-ray diffraction (XRD) pattern were obtained by a Bruker diffractrometer (D8-Advance) using $Cu_{K\alpha}$ radiation (λ=1.5418 Å). The surface morphologies of the B-γ-$CsSnI_3$ samples prepared in different deposition sequences were carried out with a scanning electron microscope (SEM, Quanta FEG 250, FEI). The elemental composition was measured with energy-dispersive X-ray spectrum (EDS, Inca, Oxford). The absorption spectra were recorded in air using UV–Vis–NIR spectrophotometer (UV-3600, Shimadzu) in a darkroom. Raman scattering was measured with a LabRAM HR Evolution (Horiba) spectrometer excited with a 532 nm laser. For photoluminescence (PL) measurements, the 535 nm excitation light from a monochromator with Xenon lamp (50 W) as light source was focused on the sample through an optical chopper (SRS 540). The PL signal was collected with a photomultiplier (PMTH-S1-CR131) and DSP lock-in amplifier (SRS 830). The electrical properties of the films were measured by a Hall Effect system (Hall, ET-9000, Eastchanging, China). The solar cell current density versus voltage (J-V) characteristics were measured using a Keithley SourceMeter 2612 A under AM 1.5 G simulated solar illumination with an intensity of 100 mW/cm^2 (Class 3 A, San-Ei, calibrated by a NREL-traceable KG5 filtered silicon reference cell). The compliance was set at 3 mA, and the scanning step was 0.3 V/s without delay time from maximum V_{oc} to zero. The metal electrodes were measured by a mask and the device area (0.1 cm^2) was determined by the overlap of the metal electrodes.

3. Results and discussion

Scheme 1 schematically illustrates the way of accessing air-stable Cs_2SnI_6 film by a room-temperature conversion of $CsSnI_3$ film at ambient atmosphere. A stoichiometric mixture of CsI and SnI_2 of 250 nm was first alternatively deposited on the glass substrates using thermal evaporation, followed by rapid thermal annealing to activate the solid-state reaction between the two precursor layers (Fig. S1), a reported protocol named as two-step sequential deposition method [26]. Subsequently, the B-γ-$CsSnI_3$ thin film evolves automatically in air and at room temperature to Cs_2SnI_6, which generally has to undergo more than 24 h. The structure of Cs_2SnI_6 shown in Scheme 1 is a defect variant of the ABX_3-type perovskite structure adopted by the $CsSnI_3$ and $CH_3NH_3PbI_3$. In Cs_2SnI_6, half of the octahedral Sn atoms are missing, creating discrete molecular $[SnI_6]^{2-}$ octahedral [27]. This compound is therefore a defect variant of the perovskite structure and contains Sn^{4+} ions rather than the extended Sn^{2+}-containing structure of $CsSnI_3$..

In the step of solid state reaction between CsI and SnI_2, the optimal temperature at 230 °C could lead to a uniform and compact orthorhombic B-γ-$CsSnI_3$ film with black luster (Fig. S2), while the preferred film growth orientation is different and dependent on the CsI and SnI_2 film deposition order, as shown in Fig. 1(a) and (b). Both the as-grown $CsSnI_3$ perovskite films have homogeneous and continuous surface coverage on the substrates, with remarkable grain size up to micrometer (Fig. 1(a) and (b), insets). The $CsSnI_3$ perovskite thin films all show strong absorption band edges starting from 950 nm and near-bandgap PL peaks with small Stokes shifts as shown in Fig. 1(c) and (d), matching well with the band gap of B-γ-$CsSnI_3$ (1.3–1.4 eV), which is also consistent with the quasiparticle self-consistent GW electronic structure calculations [21] and recent experimental data [20,25,28]..

Moreover, the electrical properties of such fresh $CsSnI_3$ thin films were investigated with the Hall effect measurements using the van der Pauw geometry, as shown in Table 1. The sign of the Hall constant is always positive and both films behave as p-type semiconductors with hole mobilities of ~120 cm^2 V^{-1} s^{-1} and 4 cm^2 V^{-1} s^{-1} for CI/SI and SI/CI film, respectively. The SI/CI film is more polycrystalline with more grain boundaries and electronic traps, which cause serious scattering, reducing the carrier mobility. This has been proved to be an important effect in poly-silicon for solar cells [29]. The CI/SI film exhibits a typically comparable data with other p-type semiconductors with similar band gap like GaAs (1.45 eV, 400 cm^2 V^{-1} s^{-1}) [30]. Their carrier concentrations

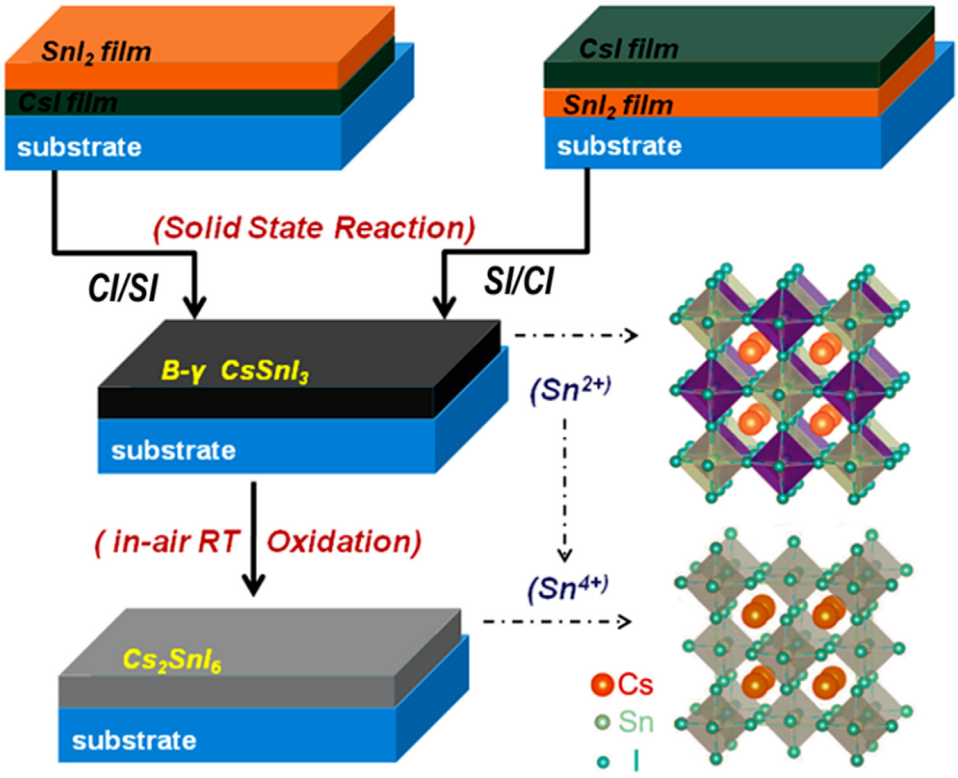

Scheme 1. Schematic illustration of the growth of Cs_2SnI_6 film from $CsSnI_3$ via a two-step deposition method based on solid state reaction. The perovskite crystal structures of Cs_2SnI_6 and $CsSnI_3$ are also shown.

of the CI/SI and SI/CI films were measured to be 6.6×10^{18} cm^{-3} and 8.4×10^{17} cm^{-3}, respectively, which are lower than that of solution-grown $CsSnI_3$ films [25] and comparable to that of the melt grown ingots [20], see Table 1. Recently, primary solar cell results using the solution-grown $CsSnI_3$ film as light absorber indicate that the high carrier density can cause serious photocarrier recombination resulting in small open-circuit voltage and low photovoltaic efficiency [25]. So, controlling the carrier density of perovskite film is important for solar cell application. Moreover, as the carrier concentration of $CsSnI_3$ is associated with the intrinsic Sn-cation vacancy defects, such low carrier densities indicate that these two-step vapor phase deposited $CsSnI_3$ films exhibit high semiconducting quality with low-density intrinsic defects.

However, it is found that these as-obtained B-γ-$CsSnI_3$ films begin to degrade fairly rapidly when they were exposed to air, which could be directly visualized via optical photographs (Fig. 2 (a) and (b)). The color changes after a few minutes indicate rapid degradation of both CI/SI and SI/CI films. With exposure time increasing, the color converts gradually from black to yellow, and finally to light black again after 24 h. XRD measurements were carried out to better understand the color change observed from the B-γ-$CsSnI_3$ perovskite films at the ambient atmosphere (Fig. 2 (c) and (d)). After exposing the perovskite thin films to air for half an hour, the yellow (Y)-phase $CsSnI_3$ was observed from both films together with a small amount of its B-γ phase and SnO_2, which agrees with the yellow and black colors of the films. The CI/SI film contains more B-γ $CsSnI_3$ component compared with the SI/CI film, which confirms its better stability in air. Some new diffraction peaks denoted by stars, spades, and circles emerge. After 24 h, both films return to black color. The new diffraction peaks (Fig. 2 (d)) with stars at 13.1°, 26.5°, 30.7°, and 44.0° can be attributed to the (111), (222), (004) and (044) lattice planes of Cs_2SnI_6, which is a rarely reported compound semiconductor [31]. Furthermore, several diffraction peaks at 27.6°, 48.7°, 56.9°, 64.7°, and 65.9° assigned to CsI, SnI_2, and SnO_2 are also observed. When keeping longer at room temperature in air, the XRD peaks of Cs_2SnI_6 films in Fig. 3(a) become more distinct while the XRD peaks of the CsI and SnI_2 film become weak. Several days later, relative pure Cs_2SnI_6 with trace amounts of SnO_2 was observed, which reveals its air-stable feature of Cs_2SnI_6. Unlike the newly synthesized B-γ-$CsSnI_3$ perovskite thin films whose orientations are dependent on the CsI/SnI_2 film deposition order, the Cs_2SnI_6 films are almost without preferred growth orientation...

Accordingly, the absorption intensity of B-γ-$CsSnI_3$ began to decrease rapidly after exposing to air for half an hour as shown in Fig. 3(b), and new absorption edges at 2.55 eV (480 nm) and 1.48 eV (840 nm) appear for the degenerative $CsSnI_3$ film, indicating the formation of its Y-phase (Eg ~ 2.5 eV) [20] and a new phase, Cs_2SnI_6, with an optical band gap of 1.48 eV (more discussion below). The coexistence of both two absorption band edges is thus due to the partial conversion of B-γ-$CsSnI_3$ film to its Y-phase. Then, the absorption intensity of Cs_2SnI_6 film increases quickly and the absorption bandedge of Y-$CsSnI_3$ film disappears gradually. After several days, only the absorption edge from the Cs_2SnI_6 film is observed, whose phase is further confirmed by the Raman spectrum (Fig. 4(a)). The $[SnI_6]^{2-}$ octahedra in Cs_2SnI_6 has six typical symmetric stretching vibration modes (ν_1–ν_6), among which ν_1, ν_2, and ν_5 modes are Raman-active, which are all observed here [32]. But the ν_5 mode at very low wave number is a little different to the pure theoretical prediction [33]..

As analysised via the above XRD data, partial CsI, SnI_2, and SnO_2 peaks were observed during the $CsSnI_3$ film envolution process. Based on these findings, the chemical reactions involved may as follows:

$$CsSnI_3 \rightarrow CsI + SnI_2 \quad (1)$$

$$2CsI + 2SnI_2 + O_2 \rightarrow Cs_2SnI_6 + SnO_2 \quad (2)$$

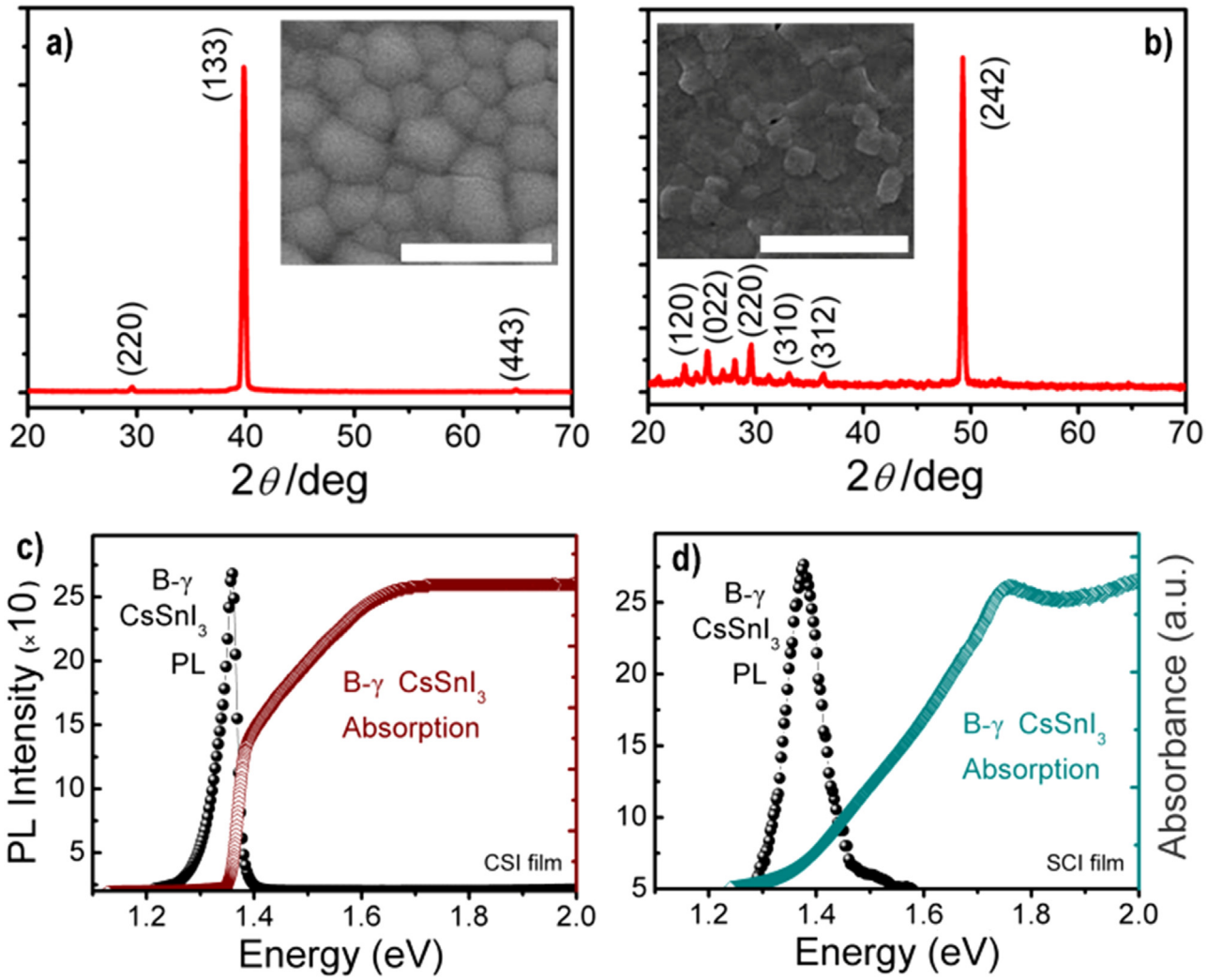

Fig. 1. (a, b) B-γ-$CsSnI_3$ perovskite films were grown through reaction between CsI and SnI_2 films at 230 °C in N_2 with different deposition order. XRD patterns and surface SEM images (insets, scale bar 4 μm) of (a) CI/SI and (b) SI/CI thin films. (c, d) Optical absorption and photoluminescence spectra of newly synthesized B-γ-$CsSnI_3$ thin films indicating a direct bandgap of about 1.3 eV, (c) CI/SI film, (d) SI/CI film.

Table 1
Electrical properties from a batch of B-γ-$CsSnI_3$ films measured with the Hall Effect. Additional data are also presented for solution-grown films and polycrystalline ingots for comparison.

Physical Properties	CI/SI thin film	SI/CI thin film	Solution-grown film[25]	Polycrystalline ingots[20]
Carrier density (cm^3)	6.6×10^{18}	8.4×10^{17}	3.05×10^{19}	$< 10^{17}$
Mobility ($cm^2\ V^{-1}\ s^{-1}$)	120	4	20	585
Resistivity (ohm cm)	0.01	1.93	0.01	0.90
Conduction type	P	P	P	P

Therefore, an overall balanced reaction for the conversion will be,

$$2CsSnI_3 + O_2 \rightarrow Cs_2SnI_6 + SnO_2 \quad (3)$$

The high instability of $CsSnI_3$ film in air derives from the inherent tendency of Sn^{2+} ions to oxidize [34]. The Sn^{2+} ion is considerably sensitive to the external oxygen, and it will be oxidized to its more stable Sn^{4+} analog, especially under a moisture environment. This oxidation process will essentially destroy the charge neutrality of the $CsSnI_3$ perovskite structure and thus cause it to decompose. Interestingly, as a defect variant of the perovskite structure, half of the octahedral Sn atoms are missing in the more-stable Cs_2SnI_6, which creates discrete molecular $[SnI_6]^{2-}$ octahedra, as shown in Scheme 1.

For solar cell application, according to the detailed balance limit of efficiency [35], the light absorber have to possess a suitable band gap (1.0–1.6 eV) that would maximize solar cell efficiency and high absorption coefficient that match well with the solar spectrum [36]. As shown in Fig. 4(b), Cs_2SnI_6 exhibits a remarkably sharp absorptance onset at a photon energy of ~1.48 eV, with a rising absorptance until a shoulder appears at larger photon energy, following which it saturates for photon energies above ~1.80 eV. Near this absorptance onset at 1.45–1.55 eV, the absorption spectrum features a fast increase. By combining its PL spectrum together (Fig. 4(b)), the direct optical bandgap of 1.48 eV of Cs_2SnI_6 is accurately estimated. It is slightly larger than the formerly reported data by only measuring the optical diffuse reflectance spectrum of Cs_2SnI_6 ingots (1.26 eV) [31]. Most recently, Saparov et al. grew Cs_2SnI_6 film by evaperating CsI and then annealing it in SnI_4 vapor and measured a optical bandgap of 1.62 eV. But, their calculated data also indicated that the Cs_2SnI_6 bandgap is in a range of 1.27–1.62 eV depending on the hybrid functional exchange data adopted [37]. The badgap of Cs_2SnI_6 is very

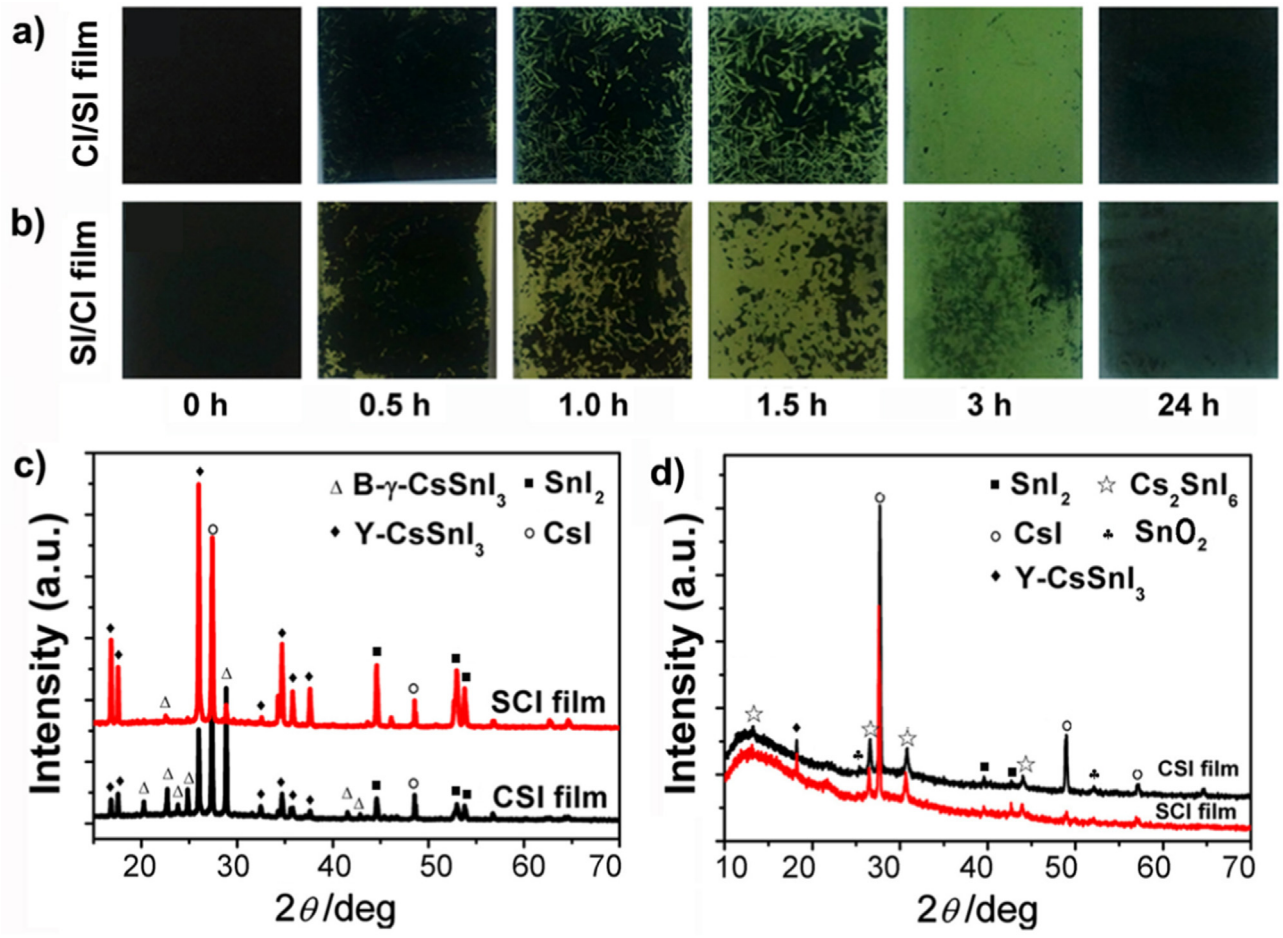

Fig. 2. (a, b) Time-dependent color changes of B-γ CI/SI and SI/CI perovskite thin films when exposed to the atmosphere from 0 to 24 h, respectively. (c, d) XRD patterns of the CI/SI film and SI/CI film corresponding to 0.5 h and 24 h. The conversion to the Cs_2SnI_6 phase is evident. (For interpretation of the references to color in this figure legend, the reader is referred to the web version of this article.)

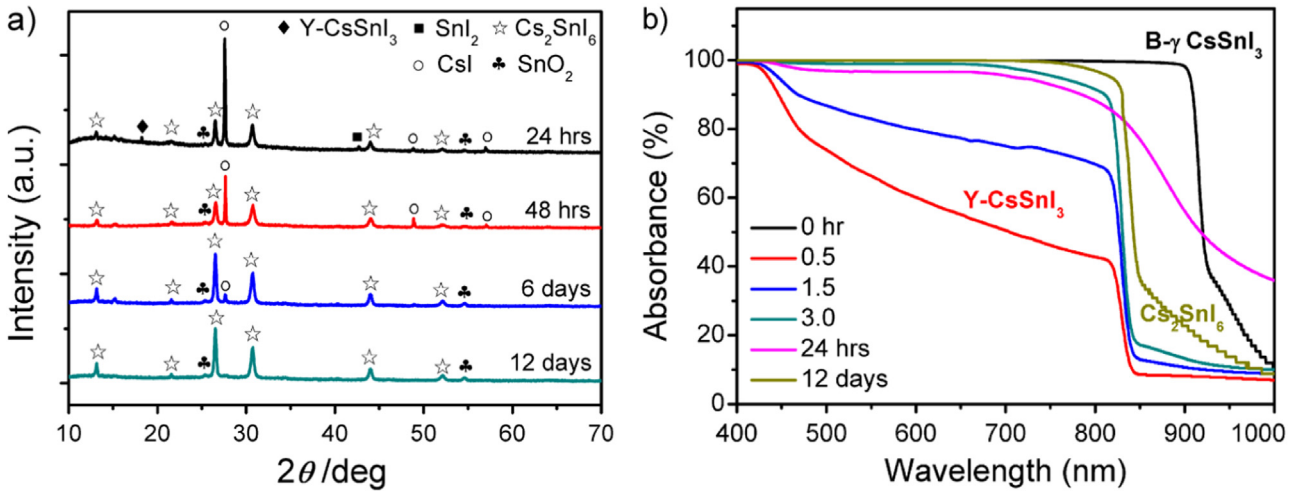

Fig. 3. (a) XRD pattern envolution of the B-γ Cs_2SnI_6 films in air after 24, 48 h, 6 days, and 12 days, (b) The absorbance spectrum evolution of a CI/SI film in air and the corresponding absorption edges labeled respectively. The absorption spectrum of SI/CI film shows similar behavior (not shown).

comparable to the badgap data of $CH_3NH_3PbI_3$ (~1.57 eV) and market-relevant CdTe (~1.51 eV) [38], which both contain toxic elements Cd and Pb. According to the Shockley-Queisser limit for the efficiency of a single-junction solar cell under unconcentrated sunlight, a theoretical maximum efficiency over 20% can be expected for Cs_2SnI_6 as light absorber [39]. Further insight into the relevance of the absorption spectrum were obtained by comparing the absorption coefficients of the Cs_2SnI_6, $CH_3NH_3PbI_3$, and CdTe films, as shown in Fig. 4(b). The curve of the Cs_2SnI_6 absorption coefficient shows an unusual sharp shoulder near its bandgap value. It is also particularly remarkable that Cs_2SnI_6 exhibits higher absorption coefficient (over 10^5 cm^{-1} from 1.7 eV) than the other two reference semiconductors in a wide solar spectrum range. This may explain why very thin Cs_2SnI_6 absorber film (~300 nm)

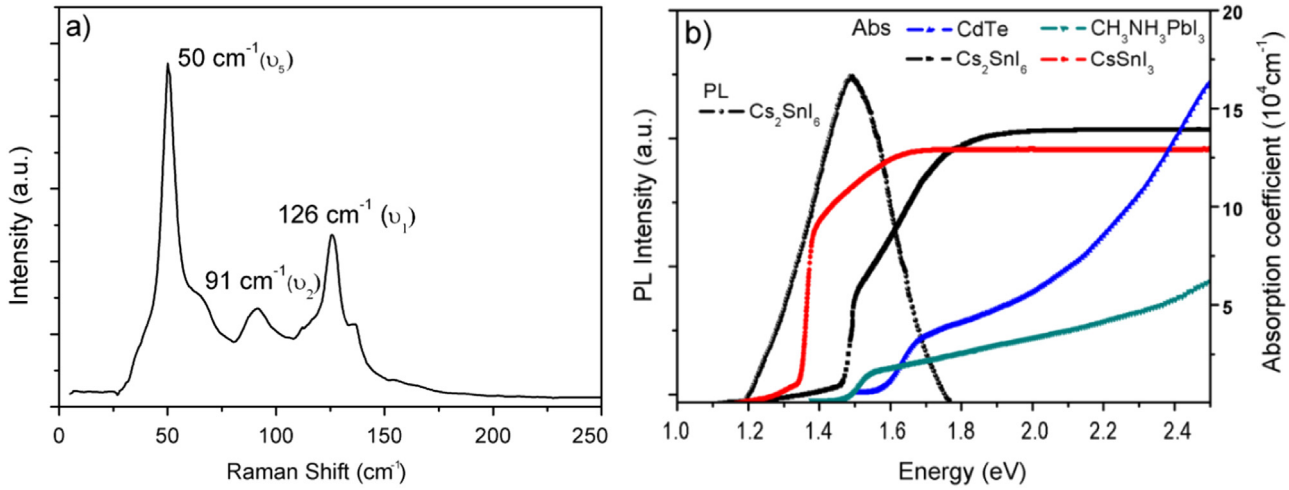

Fig. 4. (a) Raman spectrum of the Cs_2SnI_6 thin film after ten days. (b) Absorption coefficient and PL spectra (black) of Cs_2SnI_6 thin film, indicating its direct bandgap of about 1.48 eV. The absorption coefficient spectra of the as-prepared B-γ-$CsSnI_3$ thin film and other light absorbers for typical solar cells like CdTe and $CH_3NH_3PbI_3$ are also shown for comparison.

suffices for perovskite solar cell fabrication (see following part).

To further directly evaluate the photovoltaic performance of Cs_2SnI_6 as light absorber, Cs_2SnI_6 films prepared in air by the above oxidative phase conversion of B-γ-$CsSnI_3$ films were adopted for solar cell febrication with a configuration of glass/FTO/TiO_2/Cs_2SnI_6/P3HT/Ag, as shown in Fig. 5(a)–(c). FTO/glasses were used as substrates and TiO_2 thin layer as blocking layers. More details about Cs_2SnI_6 based solar cell febrication process and device structure optimization were shown in experimental section and Supporting Information. The cross-section SEM images (Fig. 5(b)) indicates a clear planar N-i-P device structure with Cs_2SnI_6 film as light-absorbing layer. The current density-voltage (J-V) characteristics of the devices utilizing Cs_2SnI_6 films of different thicknesses are displayed in Fig. 5(d) and Table S2. The best power conversion efficiency was observed for 300 nm-thick Cs_2SnI_6 film device with photovoltaic parameters $J_{sc}=5.41$ mA cm^{-2}, $V_{oc}=0.51$ V and FF=0.35, resulting in a PCE of 0.96%. Though this is the first demonstration of Cs_2SnI_6 as solar cell absorber material in air as far as we know, the relatively excellent performance already outperforms the $CsSnI_3$ based planar Schottky cell [24] and comparable to $CsSnI_3$ based mesoporous cell, which both can only work in nitrogen glove box [25]. Primarily, the cell performance enhancement mainly benefits from the improved film morphology and optimized thickness (Fig. 5(a) and (b)), but the energy-barrier mismatches between the TiO_2/perovskite/HTM layers may lead to inefficient electron/hole extractions toward the electrodes, which could contribute to the current low conversion efficiency. In addition, Hall measurements on the Cs_2SnI_6 films failed due to the very high resistivity (~MΩ), which could also result in the low fill factors of solar cells..

To test the device reproducibility, for the J-V measurements of each group devices with Cs_2SnI_6 film as absorber, 5–10 solar cells were successfully fabricated and over 30 devices were measured totally. Their optical photographs are typically shown in Fig. S4. The complete planar solar cell devices were fabricated with Cs_2SnI_6 layers of different thickness on compact-TiO_2 blocking layers using FTO glass as substrate. On top of the Cs_2SnI_6 film, P3HT was used as hole transporting layer and Ag was used as top electrical contact. Fig. S5 shows the PCE data and solar cell device numbers measured and Table S2 shows the average device PCE for each Cs_2SnI_6 layer thickness, which both indicates good device reproducibility. Moreover, as we all know, organic-inorganic hybrid perovskite solar cells usually exhibit hysteresis when the I-V scans in different directions. Our primary study shows that such inorganic Cs_2SnI_6 film solar cell also has the hysteresis phenomena (Fig. S6). Although ferroelectric, ion migration, and electrode polarizations have been proposed as a basis for the hysteresis, origin of hysteresis has not been apparently unraveled and more study is still needed even for the well-studied $CH_3NH_3PbI_3$ based perovskite solar cell [40].

Though the Cs_2SnI_6 film itself is stable upon aging in dry air (RH < 20%), we found the solar cell PCE degradation when using it as the light absorber, as shown in Fig. 5(e) and (f). This is possibly due to the material degradation upon applied bias, which usually has important implications for long-term stability [41]. Moreover, the degradation can also originate from any of the materials and materials interfaces composing the device. For examples, the organic hole transporting materials (e.g. P3HT) have been reported as one of the most problematic source of performance losses [42]. However, it is still remarkable to note that the solar cell stability measurements in air revealed a pronounced stability of the unsealed solar cells for at least one week (Fig. 5(e) and (f)). The cell PCE decreased thereafter and the device failed after about one month, the reason of which is still our ongoing task to investigate. Our future work includes as well the innate dynamics of the photoexcited electrons and holes in Cs_2SnI_6 and the fundamental properties of Cs_2SnI_6 like the electron and hole diffusion lengths, to help obtain higher efficiencies. This is the most critical question concerning whether mesostructured [43] or planar heterojunction (in this paper) perovskite solar cells will eventually dominate the device structure.

4. Conclusion

In conclusion, we have demonstrated the growth of air-stable Cs_2SnI_6 film from the oxidative conversion of unstable B-γ-$CsSnI_3$ and adopted the Cs_2SnI_6 film for the first time as a light absorber for planar lead-free perovskite solar cell. It was proposed that the instability of $CsSnI_3$ film in air due to the inherent instability of Sn^{2+} ions results in a fast phase change to its oxidation state of Cs_2SnI_6. Importantly, the air-stable Cs_2SnI_6 with a bandgap of 1.48 eV and high absorption coefficient (over 10^5 cm^{-1} from 1.7 eV) can be utilized as an effective light absorber material in a simple planar N-i-P solar cell structure, and a preliminary encouraging energy conversion efficiency of near 1% in air was obtained. The pronounced stability of Cs_2SnI_6 at ambient atmosphere and the stable conversion efficiency of unsealed Cs_2SnI_6 solar cell over one week is highly expected to trigger further exploitation of

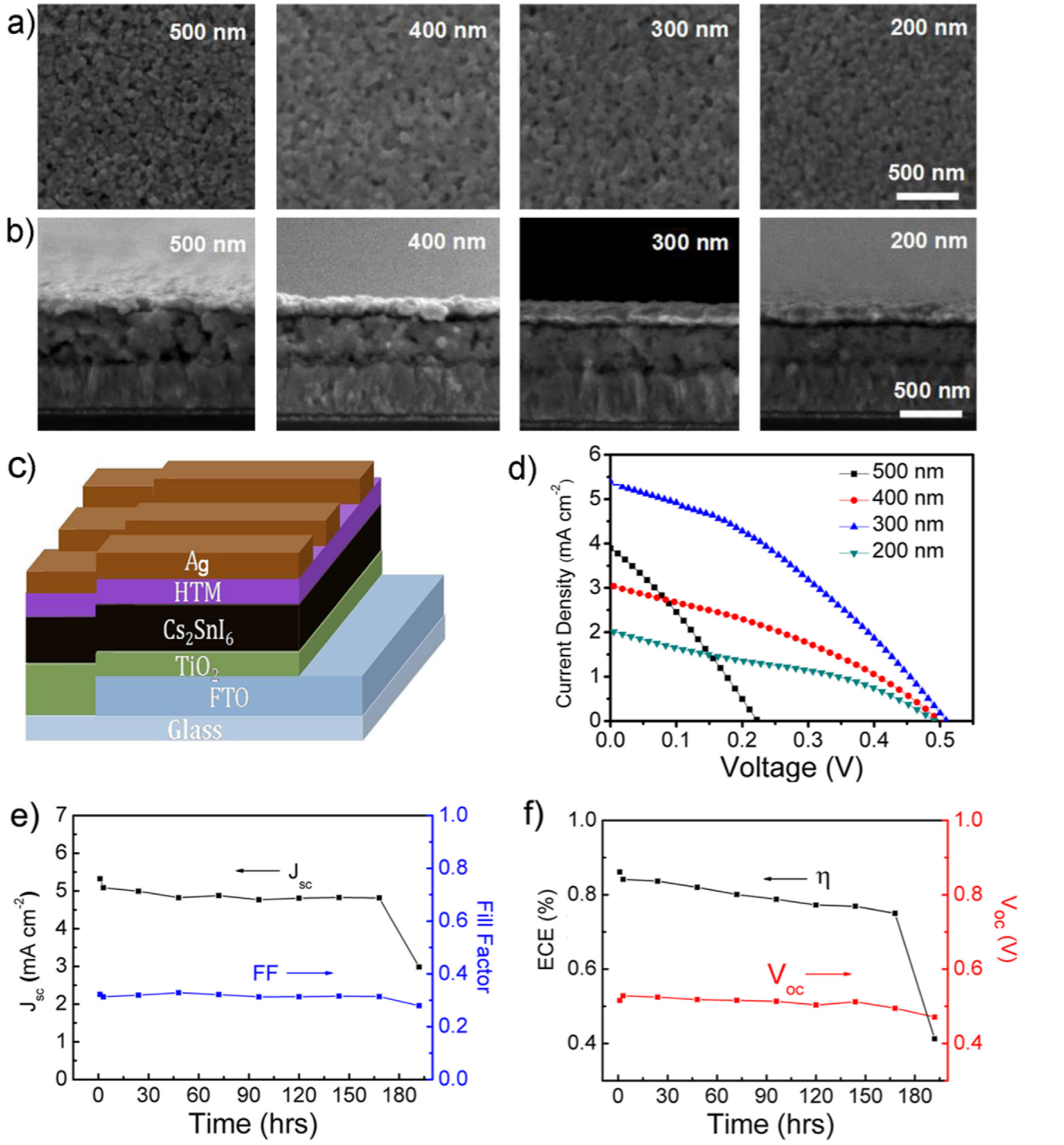

Fig. 5. (a, b) Top view and cross-sectional SEM images of the complete planar devices, indicating the following layers: conducting FTO layer (400 nm), TiO_2 blocking layer (50 nm), Cs_2SnI_6 layer (300 nm, derived from $CsSnI_3$ film with an SI/CI deposition order) as light-absorbing layer, P3HT (50 nm) and silver (80 nm). (c) Schematic illustration of the architecture for the Cs_2SnI_6 based perovskite solar cell. (d) J-V curves of perovskite solar cells fabricated with Cs_2SnI_6 of different thicknesses. (e, f) Cs_2SnI_6-based unsealed perovskite solar cell stability measurement of the main parameters as a function of time taken at specific time intervals.

new opportunities to obtain highly desirable lead-free Cs_2SnI_6 films for perovskite solar cells with high efficiency and pronounced stability via materials and devices engineering.

Acknowledgments

This work is supported by NSFC (51472110) and Natural Science Foundation of Shandong Province (JQ201214, 2014ZRB01A47). HQW acknowledges the support from Marie Curie Intro-European Fellowship and the 1000 Youth Talents Plan of China. HBZ acknowledges the support from National Basic Research Program of China (2014CB931700). Work at Northwestern University was supported by the ANSER Center, an Energy Frontier Research Center funded by the U.S. Department of Energy, Office of Science, and Office of Basic Energy Sciences under Award Number DE-SC0001059.

Appendix A. Supplementary material

Supplementary data associated with this article can be found in the online version at http://dx.doi.org/10.1016/j.solmat.2016.09.022.

References

[1] B.V. Lotsch, New light on an old story: perovskites go solar, Angew. Chem. Int. Ed. 53 (2014) 635–637.
[2] S. Kazim, M.K. Nazeeruddin, M. Grätzel, S. Ahmad, Perovskite as light harvester: a game changer in photovoltaics, Angew. Chem. Int. Ed. 53 (2014) 2812–2824.
[3] N.J. Jeon, J.H. Noh, W.S. Yang, Y.C. Kim, S.J. Ryu, S.I. Seo, Compositional engineering of perovskite materials for high-performance solar cells, Nature 517 (2015) 476–480.
[4] J. Burschka, N. Pellet, S.J. Moon, R. Humphry-Baker, P. Gao, M.K. Nazeeruddin, M. Grätzel, Sequential deposition as a route to high-performance perovskite-sensitized solar cells, Nature 499 (2013) 316–319.
[5] J. Shi, Y. Luo, H. Wei, J. Luo, J. Dong, S. Lv, J. Xiao, Y. Xu, L. Zhu, X. Xu, H. Wu, D. Li, Q. Meng, Modified two-step deposition method for high-efficiency TiO_2/$CH_3NH_3PbI_3$ heterojunction solar cells, ACS Appl. Mater. Interfaces 6 (2014) 9711–9718.
[6] S.D. Stranks, P.K. Nayak, W. Zhou, T. Stergiopoulos, H.J. Snaith, Formation of thin films of organic–inorganic perovskites for high-efficiency solar cells, Angew. Chem. Int. Ed. 54 (2015) 3240–3248.
[7] W. Nie, H. Tsai, R. Asadpour, J.C. Blancon, A.J. Neukirch, G. Gupta, J.J. Crochet, M. Chhowalla, S. Tretiak, M.A. Alam, H.L. Wang, A.D. Mohite, High-efficiency solution-processed perovskite solar cells with millimeter-scale grains, Science 347 (2015) 522–525.
[8] H. Chen, X. Pan, W. Liu, M. Cai, D. Kou, Z. Huo, X. Fang, S. Dai, Efficient panchromatic inorganic–organic heterojunction solar cells with consecutive charge transport tunnels in hole transport material, Chem. Commun. 49 (2013) 7277–7279.
[9] A. Kojima, K. Teshima, Y. Shirai, T. Miyasaka, Organometal halide perovskites as visible-light sensitizers for photovoltaic cells, J. Am. Chem. Soc. 131 (2009) 6050–6051.
[10] H.S. Kim, C.R. Lee, J.H. Im, K.B. Lee, T. Moehl, A. Marchioro, S.J. Moon, R. Humphry-Baker, J.H. Yum, J.E. Moser, M. Grätzel, N.G. Park, Lead iodide perovskite sensitized all-solid-state submicron thin film mesoscopic solar cell with efficiency exceeding 9%, Sci. Rep. 2 (2012) 00591.
[11] M.M. Lee, J. Teuscher, T. Miyasaka, T.N. Murakami, H.J. Snaith, Efficient hybrid solar cells based on meso-superstructured organometal halide perovskites, Science 338 (2012) 643–647.
[12] S.K. Yang, J.H. Noh, N.J. Jeon, Y.C. Kim, S. Ryu, J. Seo, S.I. Seok, High-performance photovoltaic perovskite layers fabricated through intramolecular exchange, Science 348 (2015) 1234–1237.
[13] J.P. Wang, N.N. Wang, Y.Z. Jin, J.J. Si, Z.K. Tan, H. Du, L. Cheng, X.L. Dai, S. Bai, H. P. He, Z.Z. Ye, M.L. Lai, R.H. Friend, W. Huang, Interfacial control toward efficient and low-voltage perovskite light-emitting diodes, Adv. Mater. 27 (2015) 2311–2316.
[14] D.D. Zhang, S.W. Eaton, Y. Yu, L. Dou, P.D. Yang, Solution-phase synthesis of cesium lead halide perovskite nanowires, J. Am. Chem. Soc. 137 (2015) 9230–9233.
[15] G. Nedelcu, L. Protesescu, S. Yakunin, M.I. Bodnarchuk, M.J. Grotevent, M. V. Kovalenko, Fast anion-exchange in highly luminescent nanocrystals of cesium lead halide perovskites ($CsPbX_3$, X=Cl, Br, I), Nano Lett. 15 (2015) 5635–5640.
[16] Y. Wang, X.M. Li, J.Z. Song, L. Xiao, H.B. Zeng, H.D. Sun, All-inorganic colloidal perovskite quantum dots: a new class of lasing materials with favorable characteristics, Adv. Mater. 44 (2015) 7101–7108.
[17] J.Z. Song, J.H. Li, X.M. Li, L.M. Xu, Y.H. Dong, H.B. Zeng, Quantum dot light-emitting diodes based on inorganic perovskite cesium lead halides ($CsPbX_3$), Adv. Mater. 27 (2015) 7162–7167.
[18] F. Hao, C.C. Stoumpos, D.H. Cao, R.P.H. Chang, M.G. Kanatzidis, Lead-free solid-state organic-inorganic halide perovskite solar cells, Nat. Photonics 8 (2014) 489–494.
[19] I. Borriello, G. Cantele, D. Ninno, Ab initio investigation of hybrid organic-inorganic perovskites based on tin halides, Phys. Rev. B 77 (2008) 235214.
[20] I. Chung, J.H. Song, J. Im, J. Androulakis, C.D. Malliakas, H. Li, A.J. Freeman, J. T. Kenney, M.G. Kanatzidis, $CsSnI_3$: semiconductor or metal? High electrical conductivity and strong near-infrared photoluminescence from a single material. High hole mobility and phase-transitions, J. Am. Chem. Soc. 134 (2012) 8579–8587.
[21] Y. Huang, W.R.L. Lambrecht, Electronic band structure, phonons, and exciton binding energies of halide perovskites $CsSnCl_3$, $CsSnBr_3$, and $CsSnI_3$, Phys. Rev. B 88 (2013) 165203.
[22] I. Chung, B. Lee, J. He, R.P. Chang, M.G. Kanatzidis, All-solid-state dye-sensitized solar cells with high efficiency, Nature 485 (2012) 486.
[23] J. Zhang, C. Yu, L. Wang, Y. Li, Y. Ren, K. Shum, Energy barrier at the N719-dye/$CsSnI_3$ interface for photogenerated holes in dye-sensitized solar cells, Sci. Rep. 4 (2014) 6954.
[24] Z. Chen, J.J. Wang, Y.H. Ren, C.L. Yu, K. Shum, Schottky solar cells based on $CsSnI_3$ thin-films, Appl. Phys. Lett. 9 (2012) 093901.
[25] M.H. Kumar, S. Dharani, W.L. Leong, P.P. Boix, R.R. Prabhakar, T. Baikie, C. Shi, H. Ding, R. Ramesh, M. Asta, M. Grätzel, S.G. Mhaisalkar, N. Mathews, Lead-free halide perovskite solar cells with high photocurrents realized through vacancy modulation, Adv. Mater. 26 (2014) 7122–7127.
[26] K. Shum, Z. Chen, J. Qureshi, C.L. Yu, J.J. Wang, W. Fenninger, P.N. Vockic, J. Midgley, J.T. Kenney, Synthesis and characterization of $CsSnI_3$ thin films, Appl. Phys. Lett. 9 (2010) 221903.
[27] Z.W. Xiao, Y.Y. Zhou, H. Hosono, T. Kamiya, Intrinsic defects in a photovoltaic perovskite variant Cs_2SnI_6, Phys. Chem. Chem. Phys. 17 (2015) 18900–18903.
[28] T.C. Jellicoe, J.M. Richter, H.F.J. Glass, M. Tabachnyk, R. Brady, S.E. Dutton, A. Rao, R.H. Friend, D. Credgington, N.C. Greenham, M.L. Böhm, Synthesis and optical properties of lead-free cesium tin halide perovskite nanocrystals, J. Am. Chem. Soc. 138 (2016) 2941–2944.
[39] J.Y.W. Seto, The electrical properties of polycrystalline silicon films, J. Appl. Phys. 46 (1975) 5247–5254.
[30] P.H. Holloway, G.E. McGuire, Handbook of Compound Semiconductors, Elsevier, Research Triangle Park, North Carolina, 1995.
[31] B. Lee, C.C. Stoumpos, N. Zhou, F. Hao, C. Malliakas, C.Y. Yeh, T.J. Marks, M. G. Kanatzidis, R.P. Chang, Air-stable molecular semiconducting iodosalts for solar cell applications: Cs_2SnI_6 as a hole conductor, J. Am. Chem. Soc. 136 (2014) 15379–15385.
[32] I. Wharf, D.F. Shriver, Vibrational frequencies and intramolecular forces in anionic tin-halogen complexes and related species, Inorg. Chem. 8 (1969) 914–925.
[33] K. Nakamoto, Infrared and Raman Spectra of Inorganic and Coordination Compounds, Theory and Applications in Inorganic Chemistry, 6th ed., Wiley, New Jersey 2008, pp. 221–223.
[34] C.C. Stoumpos, C.D. Malliakas, M.G. Kanatzidis, Semiconducting tin and lead iodide perovskites with organic cations: phase transitions, high mobilities, and near-infrared photoluminescent properties, Inorg. Chem. 52 (2013) 9019–9038.
[35] W. Shockley, H. Queisser, Detailed balance limit of efficiency of p-n junction solar cells, J. Appl. Phys. 32 (1961) 510–519.
[36] A.L. Fahrenbruch, R.H. Bube, Fundamentals of Solar Cells, Academic Press, New York 1983, pp. 212–243.
[37] B. Saparov, J.P. Sun, W. Meng, Z. Xiao, H.S. Duan, O. Gunawan, D. Shin, I.G. Hill, Y. Yan, D.B. Mitzi, Thin-film deposition and characterization of a Sn-deficient perovskite derivative Cs_2SnI_6, Chem. Mater. 28 (2016) 2315–2322.
[38] I.H. Calderón, Optical Properties and Electronic Structure of Wide Bandgap I-VI Semiconductors, Taylor and Francis, New York 2002, pp. 113–170.
[39] S.M. Sze, Physics of Semiconductor Devices, Wiley, New York 1969, p. 644.
[40] H.S. Kim, I.H. Jang, N. Ahn, M. Hhoi, A. Guerrero, J. Bisquert, N.G. Park, Control of I–V hysteresis in $CH_3NH_3PbI_3$ perovskite solar cell, J. Phys. Chem. Lett. 6 (2015) 4633–4639.
[41] T. Leijtens, G.E. Eperon, N.K. Noel, S.N. Habisreutinger, A. Petrozza, H.J. Snaith, Stability of metal halide perovskite solar cells, Adv. Energy Mater. 5 (2015) 1500963 (23 pages).
[42] A. Abate, S. Paek, F. Giordano, J.P. Correa-Baen, M. Salib, P. Gao, T. Matsui, J. Ko, S.M. Zakeeruddin, K.H. Dahmen, A. Hagfeldt, M. Graetzela, M.K. Nazeeruddin, Silolothiophene-linked triphenylamines as stable hole transporting materials for high efficiency perovskite solar cells, Energy Environ. Sci. 8 (2015) 2946–2953.
[43] X.F. Qiu, Y.N. Jiang, H.L. Zhang, Z.W. Qiu, S. Yuan, P. Wang, B.Q. Cao, Lead-free mesoscopic Cs_2SnI_6 perovskite solar cells using different nanostructured ZnO nanorods as electron transport layers, Phys. Status Solidi (RRL) 8 (2016) 587–591.

Supporting Information

From Unstable $CsSnI_3$ to Air-stable Cs_2SnI_6: a Lead-free Perovskite Solar Cell Light Absorber with Bandgap of 1.48 eV and High Absorption Coefficient

Xiaofeng Qiu,[a] Bingqiang Cao,[*,a] Shuai Yuan,[a] Xiangfeng Chen, [a] Zhiwen Qiu, [a] Yanan Jiang,[a]

Qian Ye,[b] Hongqiang Wang,[*,b] Haibo Zeng,[c] Jian Liu, [d] Mercouri G. Kanatzidis[*,d]

[a] Materials Research Center for Energy and Photoelectrochemical Conversion, School of Material Science and Engineering, University of Jinan, Jinan 250022, China

[b] Center for Nano Energy Materials, School of Materials Science and Engineering, Northwestern Polytechnical University, Xi'an 710072, China

[c] Institute of Optoelectronics and Nanomaterials, School of Materials Science and Engineering, Nanjing University of Science and Technology Nanjing 210094, China

[d] Department of Chemistry, Northwestern University, Evanston, Illinois 60208, United States

1. Growth optimization of $CsSnI_3$ thin films

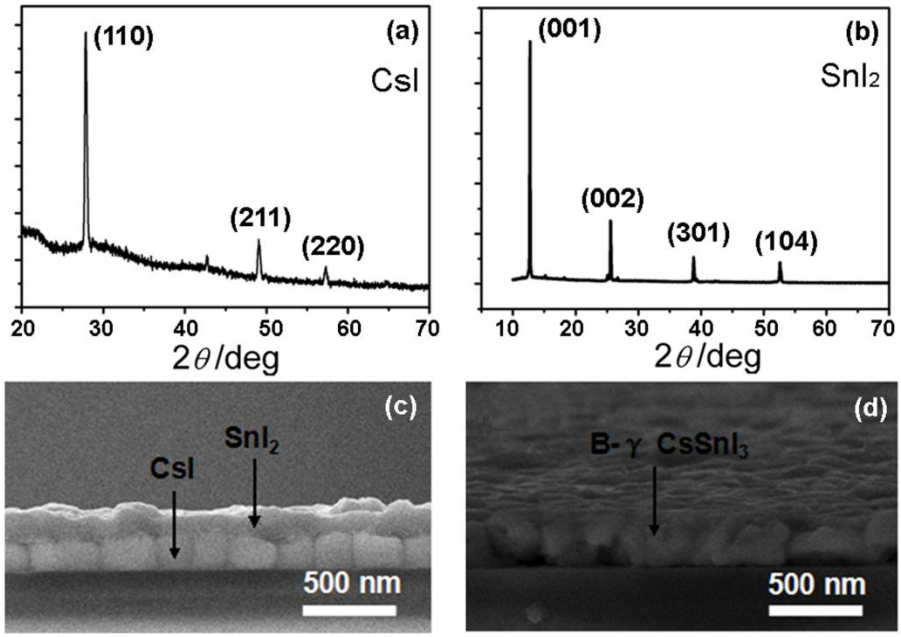

Figure S1 XRD patterns of (a) CsI and (b) SnI_2 thin films deposited on the glass substrates with thermal evaporation method. A series of typical peaks associated with respect crystal planes as labeled were obtained, indicating pure CsI and SnI_2 film were grown before depositing another layer. (c) Cross-sectional SEM images of the films before the solid-state reaction. CsI and SnI_2 layers deposited alternatively on the glass substrate by thermal evaporation; (d) B-γ $CsSnI_3$ thin film obtained via the solid-state synthesis which was facilitated through a rapid annealing treatment at 230 ^oC in N_2 atmosphere.

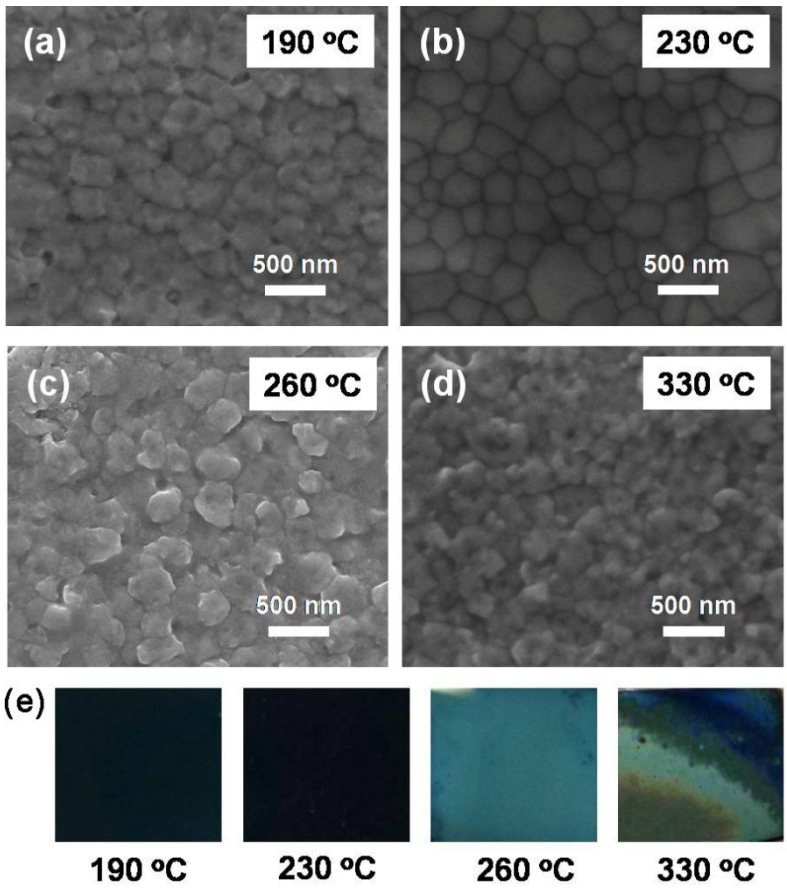

Figure S2 (a~d) SEM images and (e) corresponding optical images of B-γ-$CsSnI_3$ films grown under different solid-state reaction temperatures of 190 ºC, 230 ºC, 260 ºC, and 330 ºC, respectively. Especially, the $CsSnI_3$ sample grown at 230 ºC shows homogeneous and uniform film morphology with large grains of 100-500 nm, and no pinhole appears in entire scope. This sample was selected for planar solar cell device fabrication.

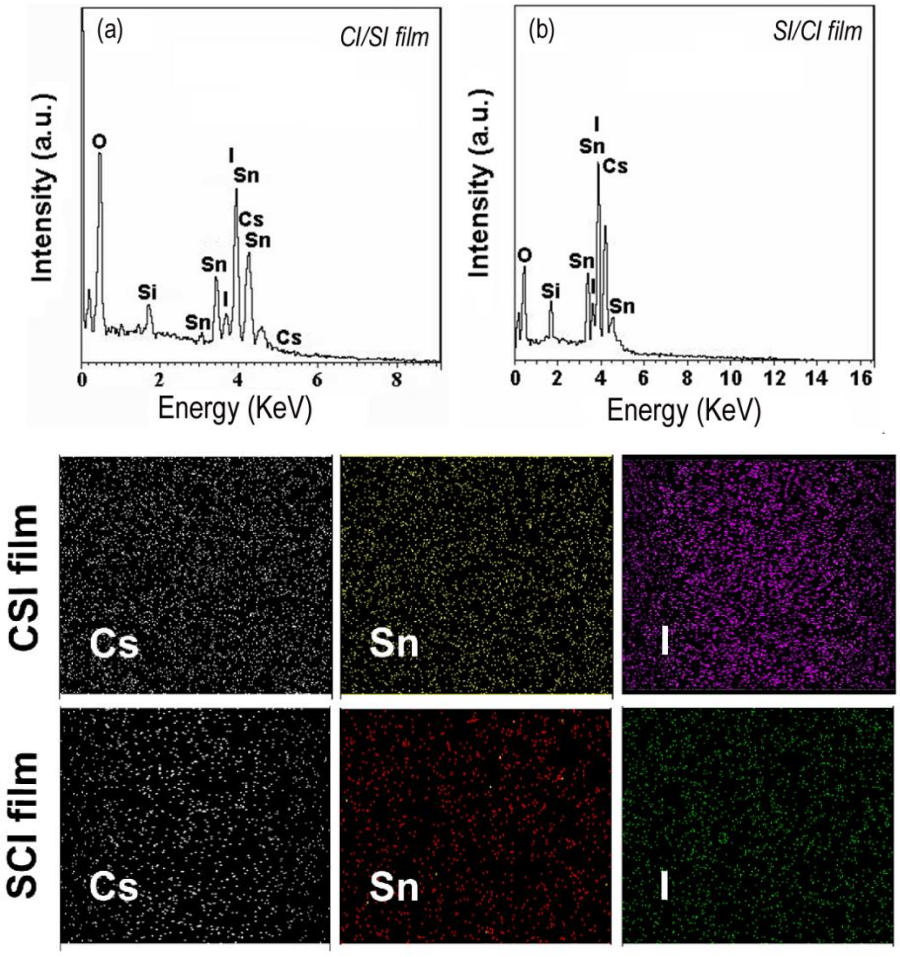

Figure S3 EDS spectra of $CsSnI_3$ samples and EDS mappings of Cs, Sn and I elements for (a) CI/SI film and (b) SI/CI thin film corresponding to insets in Fig. 1a and b. The corresponding elemental ratio analysis was shown in Table S1. The elemental analysis reveals that the Cs, Sn and I elements have an atomic ratio of nearly 1:1: 3 and the Cs, Sn and I mapping images indicate a homogeneous elemental distribution through the $CsSnI_3$ thin films.

Table S1 The elemental proportion of Cs, Sn and I analyzed from Fig. 1.

	CI/SI thin film	SI/CI thin film
Cs (%)	21.89	20.90
Sn (%)	20.16	22.00
I (%)	57.95	57.10
Atomic Ratio	1:1:3	1:1:3

2. Growth of CdTe and $CH_3NH_3PbI_3$ films for optical absorption comparison

The CdTe film was prepared on FTO substrate by electrodeposition method. Alkaline aqueous electrolyte containing 0.5 M cadmium chloride, 8 mM tellurium dioxide, and 1.5 M nitrilotriacetic acid (NTA) was prepared to electrodeposit CdTe film. The solution pH was adjusted to 9.8 with sodium hydroxide (NaOH). NTA are complexing agent for stabilizing Cd^{2+} ions. Electrochemical experiments were performed in a three-electrode cell at 80 °C under stirring with constant basic voltage at -1.0 V.

The perovskite $CH_3NH_3PbI_3$ film was deposited on glass substrate by two-step deposition method in which a mixture solution of 1:1 ratio of $PbCl_2$:PbI_2 in N,N-dimethylformamide (DMF) solvent (0.5 M) was spin-coated onto glass substrate, followed by annealing at 70 ºC for 5 min. After this step, a methylammonium iodide (MAI) solution dissolved in isopropanol (IPA) with 8mg/ml was dropped on the precursor film for 45 s (loading time), the redundant solution of MAI was removed by spinning at 4000 rpm. Finally, such film was further annealed at 70 ºC for 30 min.

References

B. B. Shan, W. B. Wu, K. Feng and H. L. Nan, Mater. Lett., 2016, 166, 85.

S. D. Stranks, P. K. Nayak, W. Zhang, T. Stergiopoulos and H. J. Snaith, Angew. Chem. Int. Ed., 2015, **54**, 2.

3. Improving the efficiency of Cs_2SnI_6 solar cell by optimizing the absorber layer morphology and thickness

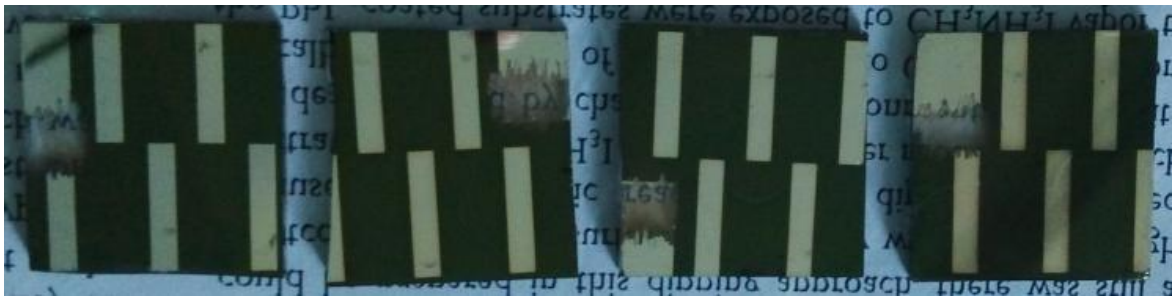

Figure S4 Optical photographs of the Cs_2SnI_6-based perovskite solar cells. The complete planar solar cell devices were fabricated with Cs_2SnI_6 layers of various thickness on compact-TiO_2 blocking layers using FTO glass as substrate. On top of the Cs_2SnI_6 film, P3HT was used as hole transporting layer and Ag was used as top electrical contact.

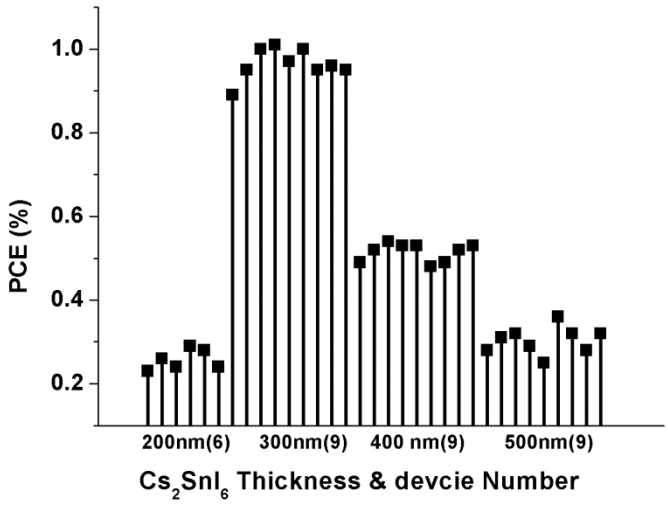

Figure S5 The PCE data of the Cs_2SnI_6-based perovskite solar cells with different thickness.

Table S2 J-V parameters of devices fabricated with different Cs_2SnI_6 thicknesses.

Sample/ parameters	J_{sc} ($mAcm^{-2}$)	V_{oc} (V)	FF	η (Ave %)
500 nm	2.03	0.49	0.30	0.31
400 nm	3.06	0.50	0.34	0.52
300 nm	5.41	0.51	0.35	0.96
200 nm	3.89	0.22	0.29	0.25

4. Current-voltage (I−V) hysteresis of the Cs_2SnI_6-based perovskite solar cells

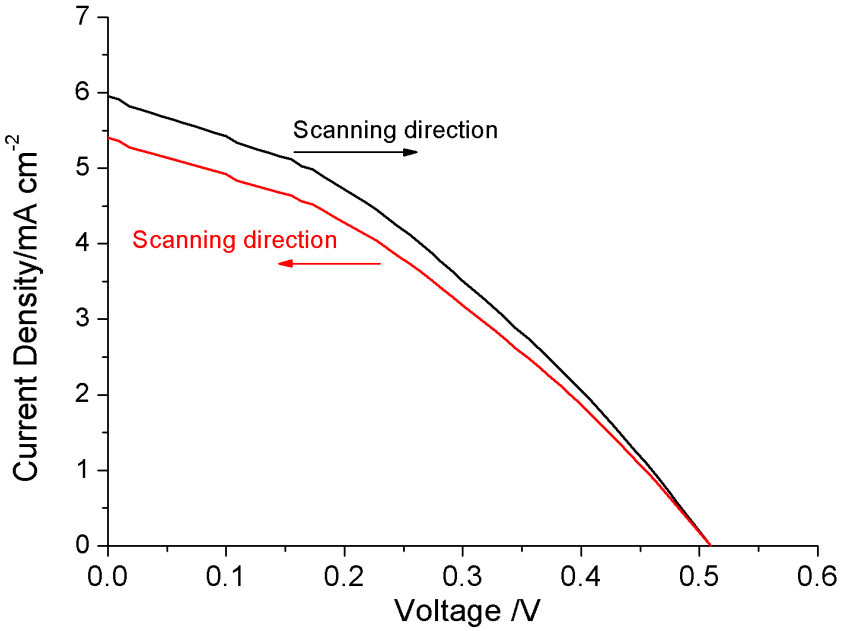

Figure S6 Scan direction-dependent I−V curves of a glass/FTO/TiO_2/Cs_2SnI_6 (300 nm)/P3HT/Ag device.